AECU-4549

UNCLASSIFIED

Physical Metallurgy of Uncommon Metals

by

John T. Norton

Robert E. Ogilvie

Date of Issue: October 15, 1959

Contract No: AT(30-1)-981

Massachusetts Institute of Technology

Cambridge, Massachusetts

UNCLASSIFIED

DISCLAIMER

Progress Report

Physical Metallurgy of Uncommon Metals

Introduction

The progress report covers the work carried out during the fiscal year 1958-59 in the department of metallurgy at M.I.T. under the supervision of Professors John T. Norton and Robert E. Ogilvie.

A brief summary of the work that has been completed and in some cases still continuing is given. The work has been listed under the following general headings:

1. Diffusion Studies in the Uranium-Niobium System
2. X-ray Detection of Cladding Defects
3. Precision X-ray Stress Analysis of Uranium and Zirconium
4. Magnetic Studies of Fe_2O_3 Single Crystals
5. Crystal Structure Studies of Yttrium Compounds
6. Structural Relationships in the $ZrFe_2$-$ZrCr_2$ System

Diffusion Studies in the Uranium-Niobium System

by Norman Peterson

The solid solubility limits of the miscibility gap in the uranium-niobium phase diagram were determined between 800°C and 1000°C by analysis of diffusion couples using an electron microbeam probe technique. A typical diffusion gradient obtained by this technique is shown in Fig. 1.

A previously unreported phase, designated hereafter as the delta phase, was found to exist along the niobium rich side of the miscibility gap. Its range of composition is from 65 to 75 atomic percent Nb at 800°C, 60 to 65 atomic percent Nb at 892°C, and about 53 to 55 atomic percent Nb at 996°C. The presence of this phase was confirmed by microhardness and metallographic analysis. The microstructure of a diffusion couple annealed for 25 days at 800°C is shown in Fig. 2. The phase diagram resulting from this work and previous work by Rogers et al is shown in Fig. 3.

Interdiffusion coefficients were determined as a function of composition and temperature for the delta phase and the high uranium $gamma_1$ phase by means of a Matano analysis of the concentration gradients obtained in the diffusion couples. The diffusion coefficients decrease with increasing niobium content in the $gamma_1$ phase. The variation of the interdifffsion coefficient, $\tilde{D}$, with temperature T, can be represented for three different compositions in the $gamma_1$ phase as follows:

$$\tilde{D}_{90 \text{ a/o U}} = 2.4 \times 10^{-6} \exp(-21,800/RT)$$

$$\tilde{D}_{95 \text{ a/o U}} = 9.6 \times 10^{-6} \exp(-23,400/RT)$$

$$\tilde{D}_{99.5 \text{ a/o U}} = 3.4 \times 10^{-5} \exp(-25,800/RT)$$

$\tilde{D}$ values were also measured for diffusion in the delta phase at 800°C and 892°C by the Matano analysis of gradients involving the phase. The values found are:

$$\tilde{D}_{800°C} = 4.13 \times 10^{-10} \text{ cm}^2 \text{ per sec at 30 a/o U}$$

$$\tilde{D}_{892°C} = 2.3 \times 10^{-10} \text{ cm}^2 \text{ per sec at 37 a/o U}$$

The presence of porosity on the uranium rich side of the diffusion couple in addition to the position of the marker interface (see Fig. 2) leads to the conclusion that the uranium atoms are diffusing more rapidly than the niobium atoms. From this information, intrinsic diffusion coefficients D_U and D_{Nb} were obtained at 99.5 atomic percent uranium. Their variation with temperature may be represented by the following relations:

$$D_U = 2 \times 10^{-4} \exp(-23,200/RT)$$

$$D_{Nb} = 3.1 \times 10^{-5} (-25\ 800/RT)$$

References

1. B. A. Rogers, D. F. Atkins, E. J. Manthon, and M. E. Kirkpatrick Trans. AIME 212 (1958) 387.

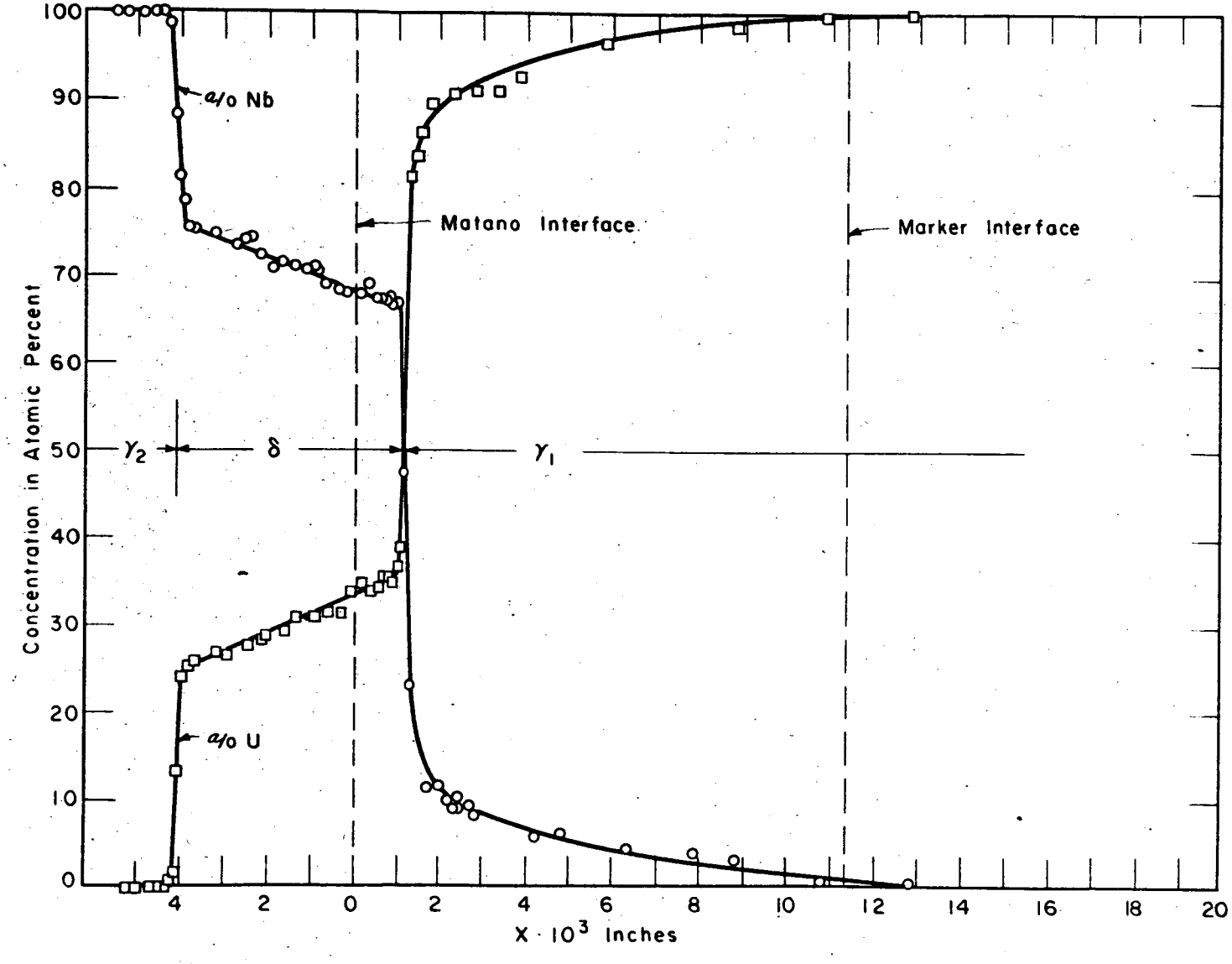

FIG. 19 URANIUM AND NIOBIUM GRADIENTS IN DIFFUSION COUPLE ANNEALED 49 DAYS AT 800°C

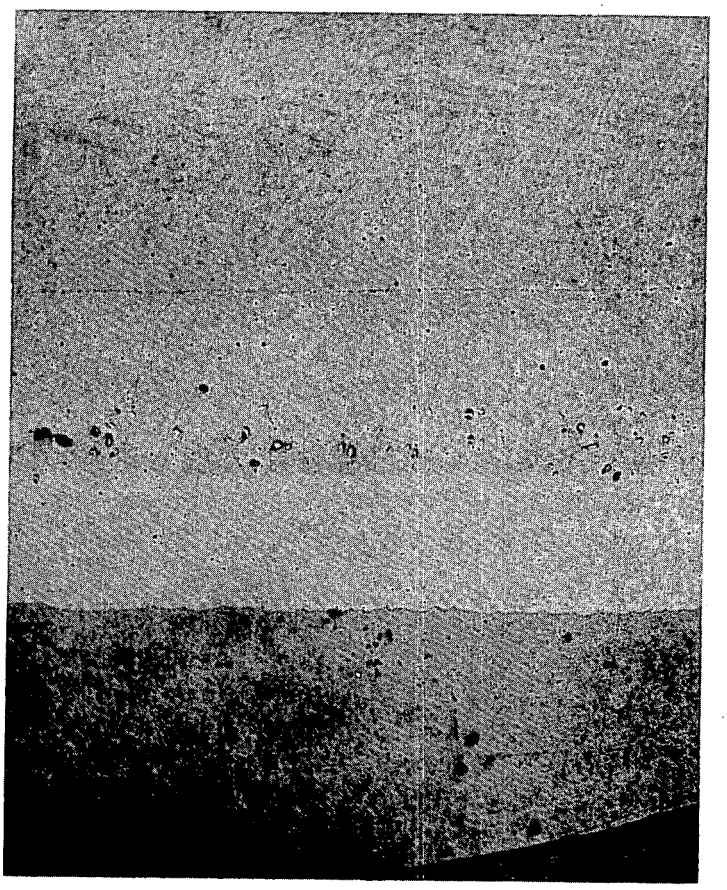

Figure 2
Microstructure of a Diffusion Couple
Annealed for 25 days at 800°C

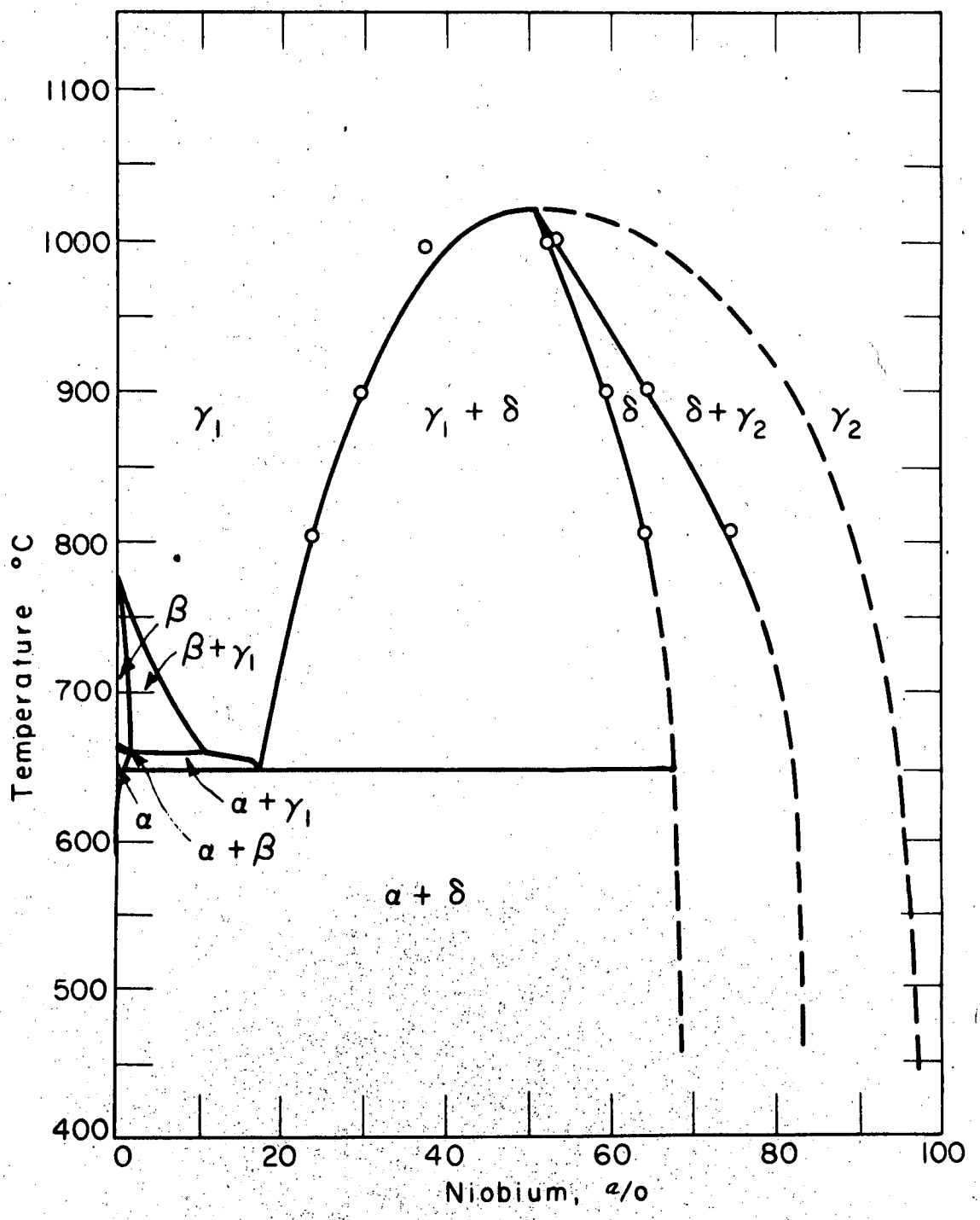

FIG. 3. PROPOSED PHASE DIAGRAM OF THE URANIUM-NIOBIUM SYSTEM

X-ray Detection of Cladding Defects

by Richard Herkner and Roy Pinkerton

The use of fluorescent x-ray attenuation as a non-destructive testing method for determining the thickness of zircalloy cladding on small diameter uranium fuel pins and the location of defects in the cladding was investigated. The initial investigation of the problem led to the choice of using the uranium $L\alpha_1$ line as the one most suited for work in this particular case.

The investigation was conducted utilizing fuel pins 0.158 inch in diameter of the type that are to be used in the Enrico Fermi power reactor. These pins have a nominal cladding thickness of 6 mils. The results show that it is possible to measure cladding thickness extremely accurately up to thicknesses of about 7 mils. Thicker clads than this reduce the intensity of the $UL\alpha_1$ to the point that it cannot be measured adequately.

The results of the investigation clearly indicate that defects in the cladding can be found in a continuous canning process.

Precision X-ray Stress Analysis of Uranium and Zirconium

Edward C. House and Bruce J. Wooden

The feasibility of using x-ray diffraction methods to measure residual stresses in uranium and zirconium (Zircalloy-2) was investigated. A precision method was developed for the determination of diffraction peak positions and the precision associated therewith. The statistical tables of Fisher and Yates were used to determine what order polynomial provided the best least squares fit within the known precision of the observed data. It was found that a second order polynomial provided an adequate regression. With the aid of a desk calculator, less than five minutes' calculation time is required to determine the peak position to a precision of $\pm$ 0.01°.

A General Electric XRD-3 Diffraction Unit was used in this investigation. The standard two-exposure method was employed in all stress measurements with the oblique position taken at 45°. Cobalt, copper and chromium radiations were investigated in determining the best high angle lines to be employed. The stress constants were determined using annealed specimens of uranium and Zircalloy-2 stressed in bending. The stress was measured with two strain gages placed one on either side of the irradiated area.

The stress constant for uranium was determined to be 1308 $\pm$ 110 psi/0.01° shift in $\Delta 2\theta$ for copper radiation on the (116) planes at $2\theta = 158.3°$. The stress constant for Zircalloy-2 was determined to be 430 $\pm$ psi/0.01° shift in $\Delta 2\theta$ for chromium radiation on the (10.4) planes at $2\theta = 156.4°$.

The surface stress distribution adjacent to the butt weld of two flat plates of Zircalloy-2 was measured. It was found that the weld produced a significant effect upon the stress distribution adjacent to the weld.

It is concluded that the expected precision as determined by statistical analysis can be attained using the method developed herein. It is recommended that a round robin specimen be sent to several stress analysis laboratories to fully verify this fact and to establish confidence in this method of residual stress measurement.

Some New Magnetic Phenomena of Hematite Single Crystals

by S. T. Lin

The magnetic properties of hematite (α - Fe_2O_3) have been a controversial problem for several decades. There are still some fundamental properties that are questionable. Hematite is primarily an antiferromagnetic material possessing a parasitic ferromagnetism. The antiferromagnetic properties have generally been agreed upon. The most controversial problems are the origin and the nature of the weak ferromagnetism above the transition temperature (about 250°K) and the existence and the nature of the weaker ferromagnetism below the transition temperature. Many authors, including the French authority L. Néel[1] believe that the weak ferromagnetism is either due to ferromagnetic impurities such as magnetite, or some type of lattice defect. Li[2], Jacobs and Bean[3] think that the weak ferromagnetism comes from the unbalanced antiferromagnetic domain walls. Neel has thought that the parasitic ferromagnetism consists of two parts, one isotropic which in independent of direction in the crystal, and the other anisotropic which tightly coupled with the direction of antiferromagnetism, which can be observed only above 250°K and in a direction perpendicular to the ternary axis. Very recently the Russian authors Dzyaloshinsky[4] and Vonsovsky[5] have developed some new theories which suggest that the weak ferromagnetism is due to the result of canted antiferromagnetism.

It seems that the confusion probably comes from the inadequacy of the experimental data. The most important single crystal data is very rare, some which is limited to a narrow range of temperature and some others to the range of the field. In order to understand the whole picture of the magnetic properties of this material it is necessary to obtain enough isotherms for a wide enough range of temperature and field along different directions of the single crystals. From these isotherms many important properties can be derived. Following this idea we have performed a great deal of experimental work and obtained a considerable amount of data which display many new results. We believe that these new results will help to solve these controversial problems.

Experimental Procedure

1. The magnetization isotherms along a certain direction in the basal plane perpendicular to the rhombohedral axis of the hematite single crystal for the temperature range from 488°K down to liquid helium temperature are obtained and shown in Figure 1. The general features of the curves are as follows: (1) At low field, the curves bend toward the field axis, (2) At high field, the curves are almost linear with field, (3) The linear portion of all the curves are almost parallel except in the transition region. These are the characteristics of a material with weak ferromagnetism superimposed on an antiferromagnetism observed in the region of small anisotropy energy. Therefore, this set of curves confirms the magnetic structure

proposed by Néel. It is to be noted that below 250°K the intercepts on the isotherms are small and that the isotherms below 250°K and above 360°K are all crowded together at their respective limiting positions. These phenomena are very significant in analyzing the isotherms.

2. The isotherms along the ternary axis which is perpendicular to the basal plane for the same temperature range as in the previous case are shown in Figure 2. These curves display a very unusual form. At temperatures well below transition, the isotherms are almost independent of magnetic field up to 15000 oersteds except at very low fields at which the curves are concave downward. Above 250°K the curves in general bend toward the field axis for low fields and then go linearly with the field. After the field reaches a certain value (critical field) it bends away from the field axis, and for still higher fields, it bends toward the field axis again. The critical field increases with decreasing temperature. The curves are also crowded together at their respective limiting positions corresponding to the temperature below 250°K and above 360°K.

From these two sets of isotherms the spontaneous magnetization, σ_o, of the weak ferromagnetism and the antiferromagnetic susceptibility X, may be separated by the usual technique of extrapolating.

Discussion

From the four curves of Figures 3 and 4, the following conclusions can be drawn:

1. Since σ_0 is practically equal to zero above 360°K in Curve 2, Fig. 4, and below 250°K in Curve 1, Fig. 4, it indicates that there is no evidence of isotropic ferromagnetism.

2. From Curve 2, Fig. 4, the anisotropic weak ferromagnetism is observable below transition (250°K) and the magnitude is above .2 emu/gm.

3. From the four curves of χ- T, and σ_0 - T, it is evident that in a wide region of over a hundred degrees the transition takes place gradually and continuously instead of rapidly and discontinuously.

4. The two curves of Fig. 4 are complementary to each other. Above 360°K $\sigma_0(111)$ (σ_0 in (111) plane) is a maximum value while σ_0 [111] (σ_0 along [111] direction) is almost zero. When the temperature decreases from 360°K to 250°K, σ_0 (111) decreased from maximum to zero while σ_0 [111] increases from zero to maximum. Below 250°K, σ_0 (111) remains zero while σ_0 [111] remains almost maximum.

5. From the statement (4) it indicates that the ferromagnetism along the ternary axis at low temperature and in the basal plane at high temperature seems to have the same nature and origin.

The above conclusions are new results which are the characteristics of the weak ferromagnetism of hematite. These characteristic phenomena are apparently contradictory to Néel's interpretation. Li's, Jacobs and Bean's proposal of unbalanced antiferromagnetic domain wall can also not explain them. However, the Russian author's proposal of canted antiferromagnetism explains the weak ferromagnetism above the transition very well, but it fails to explain the weak ferromagnetism

below the transition. In order to explain the phenomena completely a more general model of canted antiferromagnetism with unequal sublattice moments is proposed; i.e. the magnetic moment of the sublattice may tilt slightly toward each other above and in the transition region and at the same time their magnitude may differ slightly. When the temperature decreases through transition range the sublattice moments turn from the basal plane toward the ternary axis and at the same time the canted sublattice moments are gradually straightened out to become antiparallel below transition.

With this model all of the experimental data, old and new can be explained very well.

It is very interesting to note that the complementary curves of Fig. 4 can be explained completely and the complicated isotherms of Fig. 2 can also be explained satisfactorily by introducing an anisotropy energy in the crystal. The achievement of this work and the explanation of the important properties of this material are described in more detail in a paper which has been submitted to the Physical Review for publication.

References

1. L. Neel, Ann. Phys. 3, 137 (1948), 4, 249 (1949).
   L. Neel, Revs. Modern Phys. 25, 58 (1953)

2. Y. Y.Li, Phys. Rev. 101, 1450 (1956)

3. I.S. Jacobs and C. P. Bean, J. Appl. Phys. 29, 537 (1958)

4. I.E. Dzyalsohinsky, J.P.C.S. 4, 241 (1958).

5. S.V. Vonsovsky and E. A. Turov, J. Appl. Phys. 30, 98 (1959).

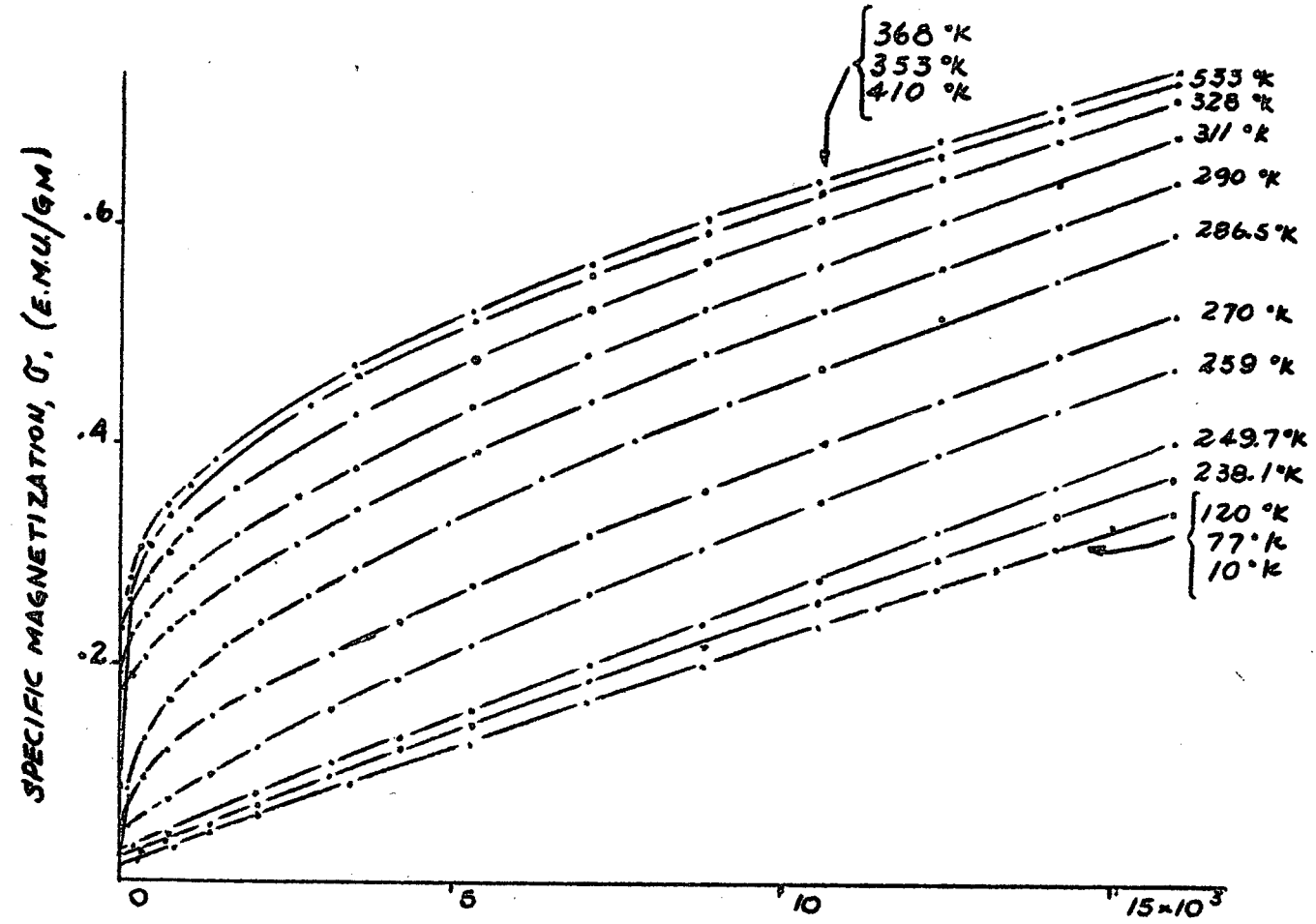

FIG 1. MAGNETIZATION ISOTHERMS OF HEMATITE SINGLE CRYSTAL ALONG A DIRECTION IN THE BASAL PLANE PERPENDICULAR TO THE TERNARY AXIS

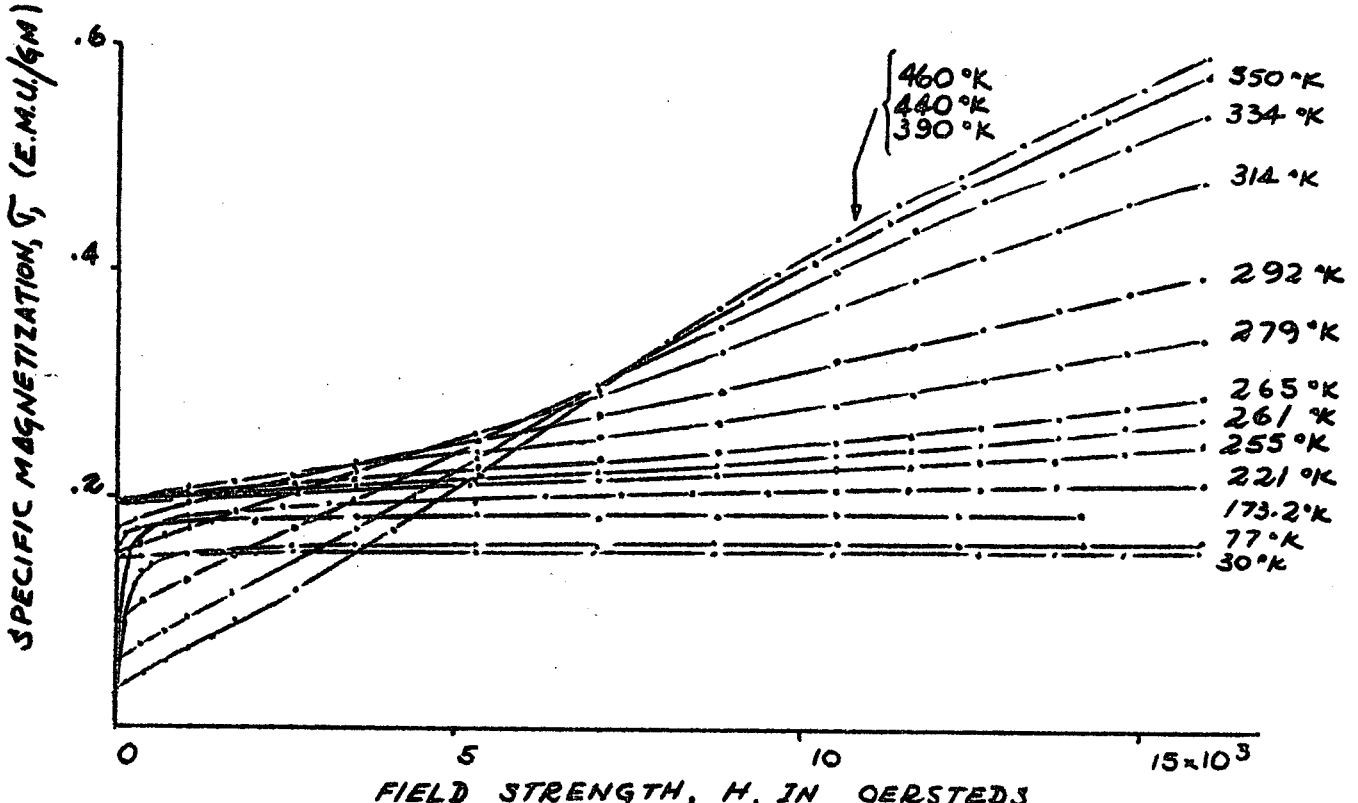

FIG 2. MAGNETIZATION ISOTHERMS OF HEMATITE SINGLE CRYSTAL ALONG THE TERNARY AXIS

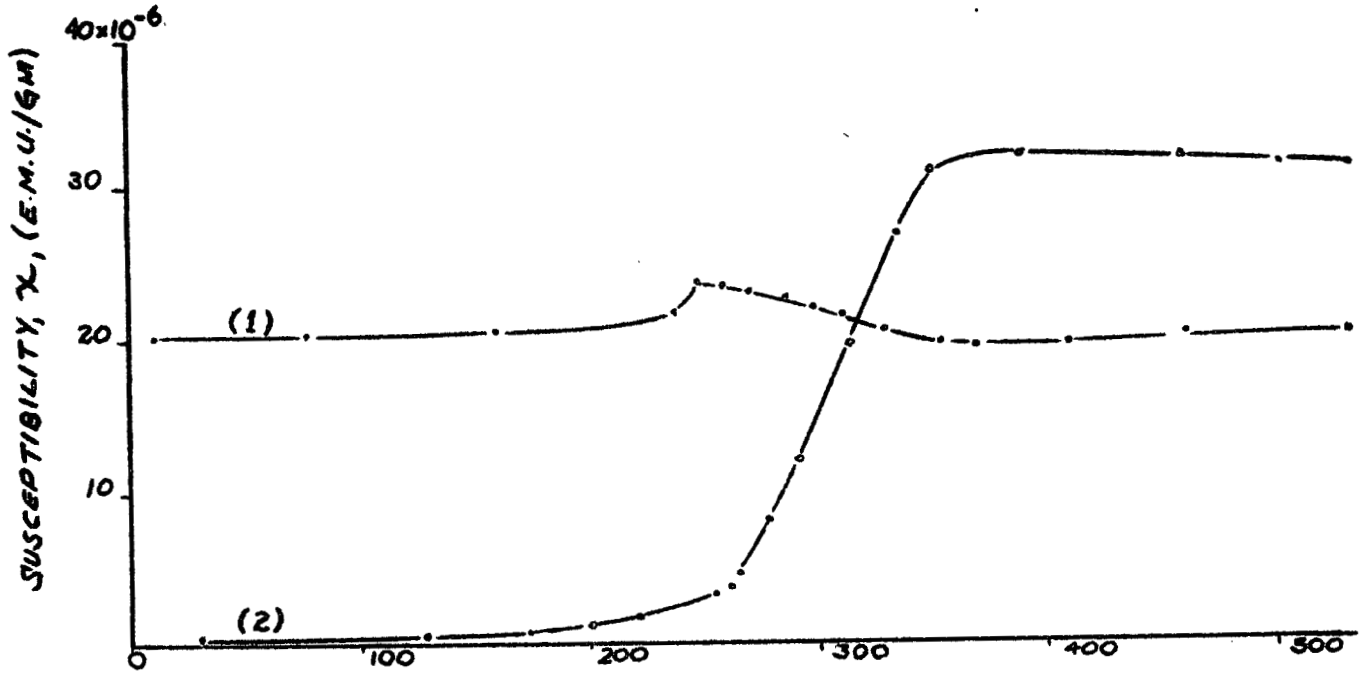

FIG 3. VARIATION WITH TEMPERATURE OF ANTIFERROMAGNETIC SUSCEPTIBILITY OF HEMATITE SINGLE CRYSTAL. (1) ALONG A DIRECTION IN THE BASAL PLANE PERPENDICULAR TO THE TERNARY AXIS, (2) ALONG THE TERNARY AXIS.

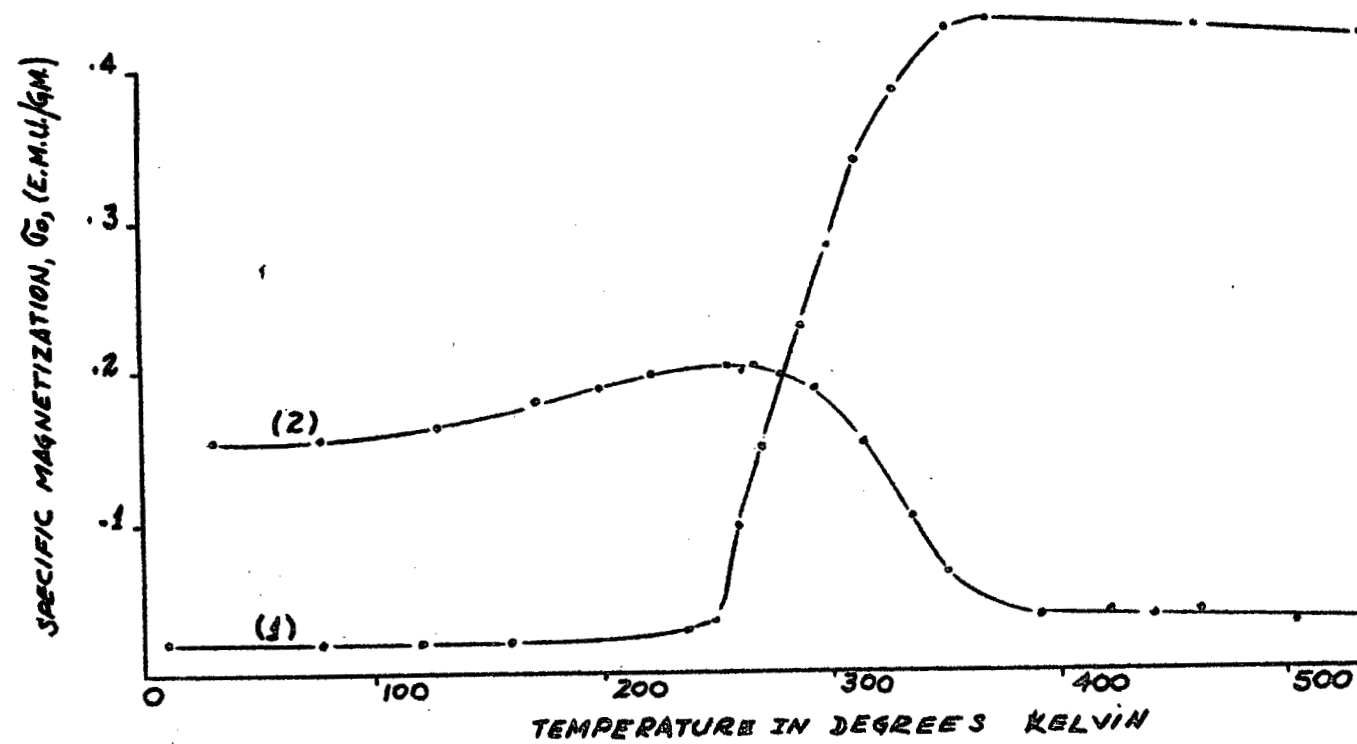

FIG 4. VARIATION WITH TEMPERATURE OF THE WEAK SPONTANEOUS MAGNETIZATION OF HEMATITE SINGLE CRYSTAL. (1) ALONG A DIRECTION IN THE BASAL PLANE PERPENDICULAR TO THE TERNARY AXIS, (2) ALONG THE TERNARY AXIS.

Crystal Structure Research

by Erwin Parthe

The progress in crystal structure research can be briefly summarized in the following two sections.

I. Crystal Structures of Yttrium Compounds

The compounds Y_5Si_3 and Y_5Ge_3 have been prepared by arc melting a mixture of the components. The molten button consisting of Y_5Si_3 contained a single crystal, which could be isolated and mounted on the goniometer head of a Weissenberg camera. The x-ray pattern of Y_5Si_3 and the isotropic Y_5Ge_3 could be indexed corresponding to a hexagonal unit cell with the constants:

Y_5Si_3	Y_5Ge_3
$a = 8.40_3$ Å	$a = 8.45$ Å
$c = 6.30_3$ Å	$c = 6.34$ Å
and $c/a = 0.75$	and $c/a = 0.75$

The extinctions lead to the possible space groups: D^3_{6h} - $P6_3/mcm$, D^2_{3h} - P6c2, C^3_{6v} - $P6_3$ cm, D^4_{3d} - P3 c1 and C^3_{3v} - P3 c1. The intensity calculation has been successful by assuming space group D^3_{6h} - $P6_3/mcm$ and placing the yttrium atoms in 4d) and $6g)_I$ with $x_I = 0.25$ and the silicon or germanium atoms in $6g)_{II}$ with $x_{II} = 0.61$.

The structure proves to be identical to the Mn_5Si_3 type, with the exception that the c/a ratio is exceptionally large. In comparison to other structures with Mn_5Si_3 type the metal atoms in $6g_I$ and in the case of Y_5Si_3 much nearer to those in 4d). This is in good agreement with what might be expected, since as in the case of Y_5Si_3 the metal atoms in $6g_I$ have to contribute electrons to the 4d metals. It is

known from an earlier developed stability criteria for Nowotny phases, that the electron concentration in 4d) has to be constant. As the yttrium atoms in 4d) cannot provide enough electrons, electrons from $6g)_I$ metal atoms have to contribute. Therefore, the a axis of the Y_5Si_3 structure is compressed which explains the exceptionally large c/a ratio.

II. A New Method to Calculate One-Dimensional Madelung Constants

From the point of view of a theoretical structure chemist it is of interest to calculate the lattice energy, more correctly the structure energy of different structures. In the case of ionic compounds it is necessary for the energy calculation to know the value of the Madelung constant. A new method of calculating one-dimensional Madelung constants has been derived.

The Madelung constant of any complicated structure can be calculated by summing up the Madelung constants of base structures. Each of these base structures has the same unit cell as the original structure but only 2 ions per unit cell. Thus the base structure consists of two simple lattice arrays occupied with ions of opposite charge. The Madelung constant of the base structure depends only on the amount these two lattice arrays are displaced from each other and the charge of the ions. Thus the Madelung constant of a base structure with ions of charge $+1_{01} - 1$ is a function of the translation parameter only and is denoted as Madelung function M(x) or M(x,y) or M(x,y,z) depending if we deal with one, two or three dimensional structures.

The one-dimensional Madelung function M(x) can be expressed by a well-known mathematical function, which is reported in the literature as $\psi(x)$ function

$$M(x) = \frac{1}{|x|} + \sum_{h=-\infty}^{h=+\infty} \left(\frac{1}{|h+x|} - \frac{1}{h}\right) \text{ omit } h + 0$$

$$= \frac{1}{|x|} - 2\gamma - \psi(x) - \psi(-x)$$

where γ is Euler's constant.

Fig. 1 shows the M(x) functions in the range from $0 < x \leq \frac{1}{2}$

As the values of the $\psi(x)$ functions are easily accessible from mathematical tables, the Madelung constant of any one-dimensional structure can be calculated to a high degree of accuracy in very short short time and without much effort.

The details of this study on the Madelung constant has been submitted to Zeitschrift fur Kristallographie.

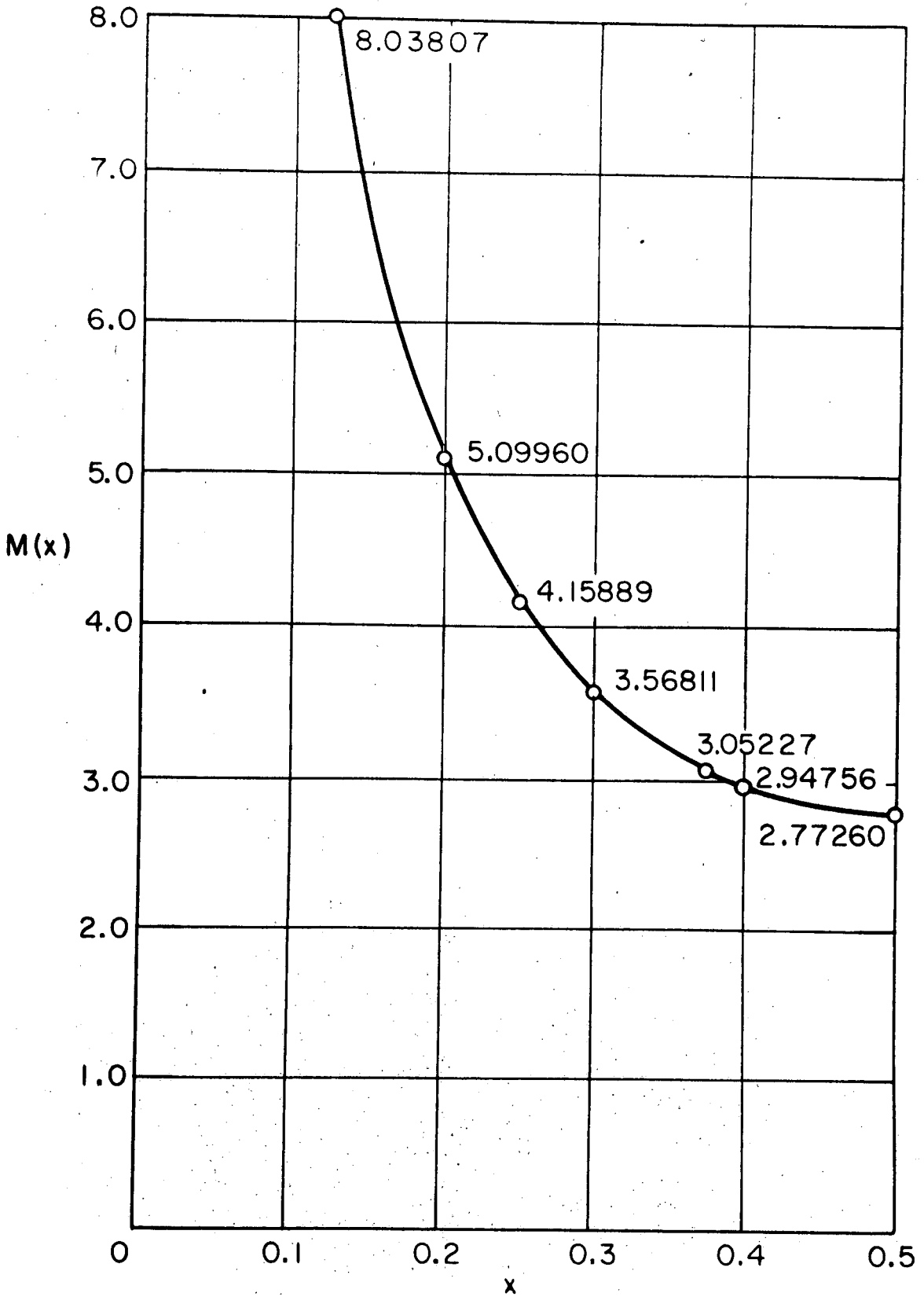

M(x) FOR CALCULATING ONE DIMENSIONAL MADELUNG CONSTANTS

Structural Relationships in the Pseudo Binary System $ZrFe_2$-$ZrCr_2$

by Simon Moss

The purpose of this work was to study by x-ray methods the solubility limits and structural identities of the phases within the pseudo binary section $ZrFe_2$-$ZrCr_2$. These phases through down done on the binary components are known to be of the Laves type AB_2. The three Laves phases are actively very similar in nature differing only in stacking sequence. Below in Figure 1 are presented the arrangements of the large atoms in the three types:

1. C14 $MgZn_2$ - hexagonal stacking: AB/AB/AB
2. C15 $MgCu_2$ - cubic (viewed only 111) stacking ABC/ABC/ABC
3. C36 $MgNi_2$ - hexagonal stacking: ABAC/ABAC/ABAC

It was known and verified here that $ZrFe_2$ is isomorphous with the cubic C15 type at all temperatures. $ZrCr_2$ has been the subject of some controversy because it exhibits allotropy. Some previous investigators have felt that $ZrCr_2$ was isomorphous with C14 at low temperatures (below 1000°C) and isomorphous with C15 above 1000°C and up to the melting point. Others have indicated that the C14 structure is stable only within a small range of temperature near the melting point and C15 is stable below this region. The present work substantiates the latter observation.

Samples intermediate between the two binary components at each 10 atom percent were solution treated at 1400°C, 1000°C and 890°C. X-ray patterns were then made of the easily crushed powder which were indexed and solved for the appropriate lattice constants.

In Figure 2 the results for the 1400°C and 890°C runs are included along with data taken on the as-quenched arc melted buttons. The phase diagram indicated is merely that which has been proposed to explain the data and has not been corroborated by additional measurements.

The results of the lattice constant, because of the structural nature of Laves phases can be applied directly to the problem of atom sizes within the compounds. Thus A-A (Zr-Zr) distances could be calculated directly from the values of the hexagonal C_{Hex} constants and the B-B (Fe,Cr-Fe, Cr) distances could be obtained from the values of A_{Hex}. These values were used to show that the transformation from cubic $ZrCr_2$ at the Cr rich end to heagonal C14 is accompanied mainly by relaxations in the A-A or Zr-Zr distortions. At the iron rich end it seems that the transformation from cubic $ZrFe_{1.8}Cr_{.2}$ to hexaongal C14 is accompanied by structural relationsions in B-B atom distances.

It also appears that the cubic structure accommodates itself to an observed radius ratio of $d_{AA}/d_{BB} = 1.225$ which is the ideal ratio for Laves phases. The hexagonal structure seems to exhibit an observed ratio slightly higher than this value for all cases.

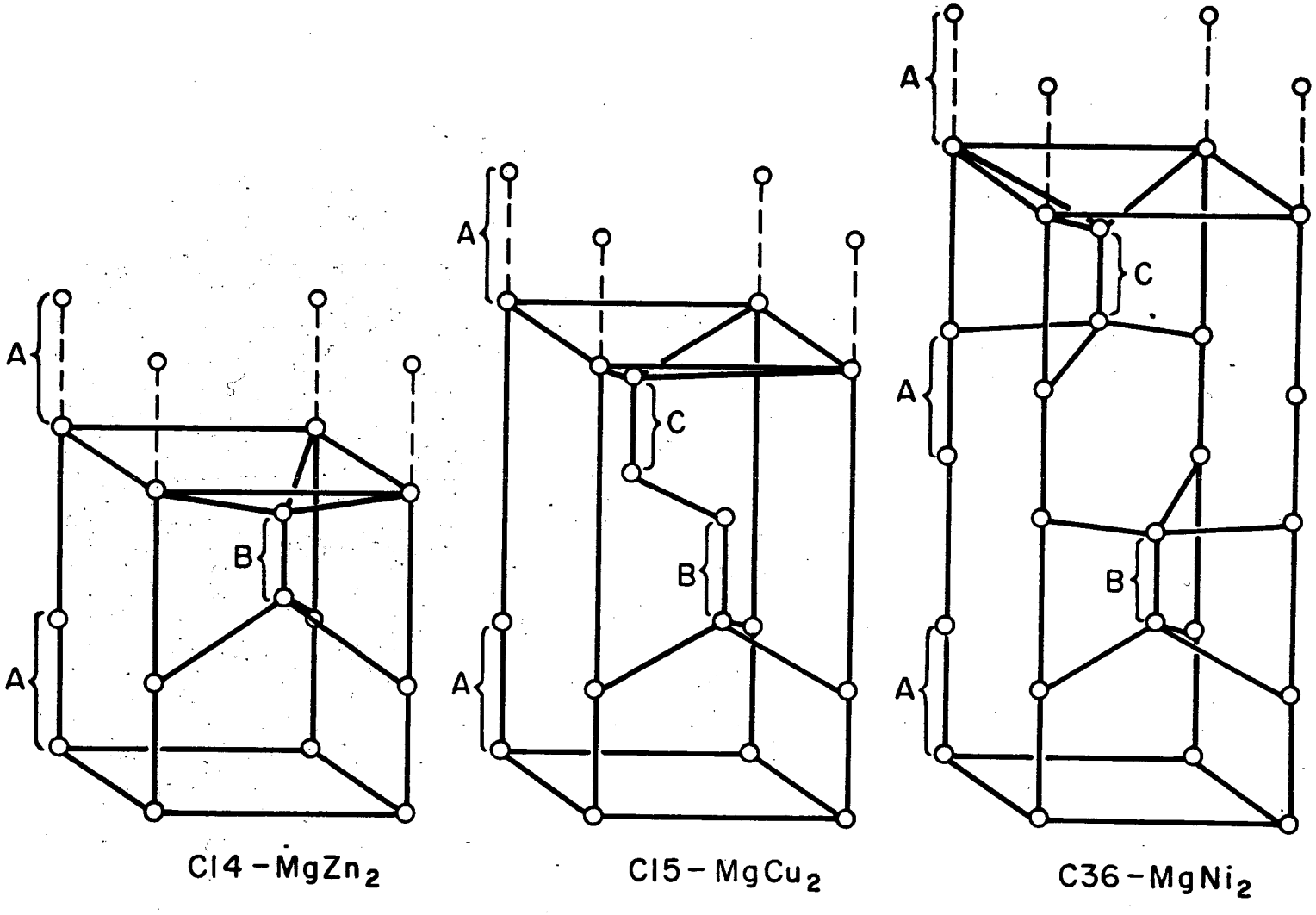

FIGURE 1 THE ARRANGEMENT OF THE LARGE A ATOMS IN THE THREE LAVES PHASES

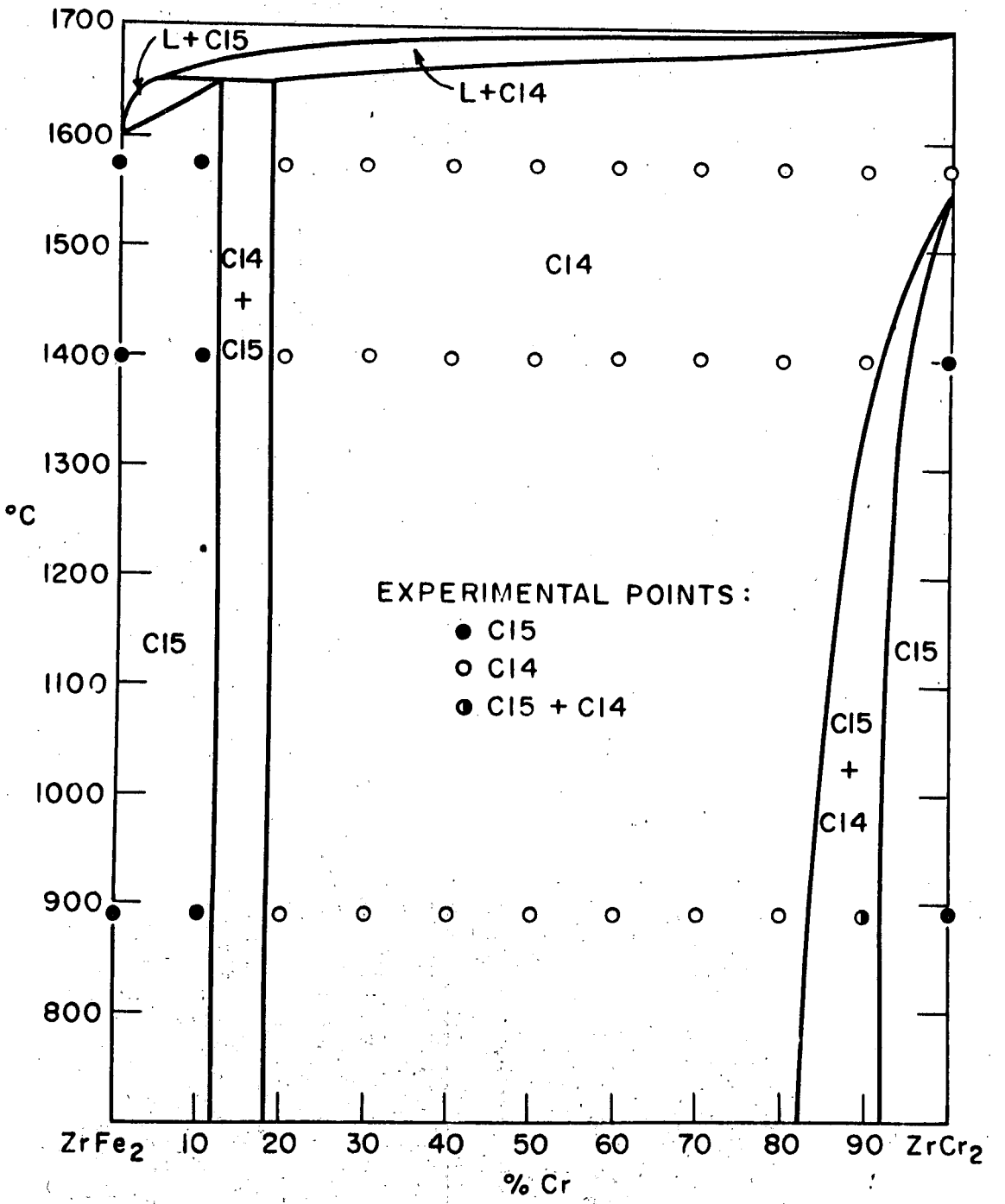

FIGURE 2 A PROPOSED PHASE DIAGRAM FOR THE PSEUDO-BINARY SECTION $ZrFe_2 - ZrCr_2$